Technical Memorandum NESS 106

AN IMPROVED MODEL FOR THE CALCULATION OF LONGWAVE FLUX AT 11 μm

Washington, D.C.
October 1979

noaa NATIONAL OCEANIC AND ATMOSPHERIC ADMINISTRATION / National Environmental Satellite Service

NOAA TECHNICAL MEMORANDUMS

National Environmental Satellite Service Series

The National Environmental Satellite Service (NESS) is responsible for the establishment and operation of NOAA's environmental satellite systems.

NOAA Technical Memorandums facilitate rapid distribution of material that may be preliminary in nature and so may be published formally elsewhere at a later date. Publications 1 to 20 and 22 to 25 are in the earlier ESSA National Environmental Satellite Center Technical Memorandum (NESCTM) series. The current NOAA Technical Memorandum NESS series includes 21, 26, and subsequent issuances.

Publications listed below are available (also in microfiche form) from the National Technical Information Service, U.S. Department of Commerce, Sills Bldg., 5285 Port Royal Road, Springfield, VA 22161. Prices on request. Order by accession number (given in parentheses). Information on memorandums not listed below can be obtained from Environmental Data and Information Service (D822), 6009 Executive Boulevard, Rockville, MD 20852.

NESS 65 Geographical Relations Between a Satellite and a Point Viewed Perpendicular to the Satellite Velocity Vector (Side Scan). Irwin Ruff and Arnold Gruber, March 1975, 14 pp. (COM-75-10678/AS)

NESS 66 A Summary of the Radiometric Technology Model of the Ocean Surface in the Microwave Region. John C. Alishouse, March 1975, 24 pp. (COM-75-10849/AS)

NESS 67 Data Collection System Geostationary Operational Environmental Satellite: Preliminary Report. Merle L. Nelson, March 1975, 48 pp. (COM-75-10679/AS)

NESS 68 Atlantic Tropical Cyclone Classifications for 1974. Donald C. Gaby, Donald R. Cochran, James B. Lushine, Samuel C. Pearce, Arthur C. Pike, and Kenneth O. Poteat, April 1975, 6 pp. (COM-75-10676/AS)

NESS 69 Publications and Final Reports on Contracts and Grants, NESS-1974. April 1975, 7 pp. (COM-75-10850/AS)

NESS 70 Dependence of VTPR Transmittance Profiles and Observed Radiances on Spectral Line Shape Parameters. Charles Braun, July 1975, 17 pp. (COM-75-11234/AS)

NESS 71 Nimbus-5 Sounder Data Processing System, Part II: Results. W. L. Smith, H. M. Woolf, C. M. Hayden, and W. C. Shen, July 1975, 102 pp. (COM-75-11334/AS)

NESS 72 Radiation Budget Data From the Meteorological Satellites, ITOS 1 and NOAA 1. Donald H. Flanders and William L. Smith, August 1975, 20 pp. (PB-246-877/AS)

NESS 73 Operational Processing of Solar Proton Monitor Data (Revision of NOAA TM NESS 49). Stanley R. Brown, September 1975, 15 pp. (COM-73-11647)

NESS 74 Monthly Winter Snowline Variation in the Northern Hemisphere From Satellite Records, 1966-75. Donald R. Wiesnet and Michael Matson, November 1975, 21 pp. (PB-248-437/6ST)

NESS 75 Atlantic Tropical and Subtropical Cyclone Classifications for 1975. D. C. Gaby, J. B. Lushine, B. M. Mayfield, S. C. Pearce, and K.O. Poteat, March 1976, 14 pp. (PB-253-968/AS)

NESS 76 The Use of the Radiosonde in Deriving Temperature Soundings From the Nimbus and NOAA Satellite Data. Christopher M. Hayden, April 1976, 19 pp. (PB-256-755/AS)

NESS 77 Algorithm for Correcting the VHRR Imagery for Geometric Distortions Due to the Earth Curvature, Earth Rotation, and Spacecraft Roll Attitude Errors. Richard Legeckis and John Pritchard, April 1976, 31 pp. (PB-258-027/AS)

NESS 78 Satellite Derived Sea-Surface Temperatures From NOAA Spacecraft. Robert L. Brower, Hilda S. Gohrband, William G. Pichel, T. L. Signore, and Charles C. Walton, June 1976, 74 pp. (PB-258-026/AS)

NESS 79 Publications and Final Reports on Contracts and Grants, NESS-1975. National Environmental Satellite Service, June 1976, 10 pp. (PB-258-450/AS)

NESS 80 Satellite Images of Lake Erie Ice: January-March 1975. Michael C. McMillan and David Forsyth, June 1976, 15 pp. (PB-258-458/AS)

NESS 81 Estimation of Daily Precipitation Over China and the USSR Using Satellite Imagery. Walton A. Follansbee, September 1976, 30 pp. (PB-261-970/AS)

(Continued on inside back cover)

NOAA Technical Memorandum NESS 106

AN IMPROVED MODEL FOR THE CALCULATION OF LONGWAVE FLUX AT 11 μm

P. G. Abel and
A. Gruber

Washington, D.C.
October 1979

UNITED STATES
DEPARTMENT OF COMMERCE
Juanita M. Kreps, Secretary

NATIONAL OCEANIC AND
ATMOSPHERIC ADMINISTRATION
Richard A. Frank, Administrator

National Environmental
Satellite Service
David S. Johnson, Director

CONTENTS

TABLES

FIGURES

AN IMPROVED MODEL FOR THE CALCULATION OF LONGWAVE FLUX AT 11 μm

P. G. Abel and A. Gruber

National Environmental Satellite Service, NOAA
Washington, D. C.

ABSTRACT. An improved method for the prediction of outgoing longwave flux from satellite radiance measurements at 11 μm is presented. The new method offers improved accuracy in estimated flux, especially at extreme flux values. It substantially reduces the discrepancy between the SR and ERB measurements, and also reduces derived outgoing longwave flux in the subtropical regions.

1. INTRODUCTION

Earth-atmosphere thermally emitted fluxes have been estimated from NOAA polar orbiting nadir window (λ = 10-12 μm) radiance measurements by application of a linear regression model. The regression coefficients were determined by using a radiative transfer model developed by Wark et al. (1962), to calculate both total emitted flux and window radiance for 100 different atmospheres, with cloudy and cloud-free conditions. The derived regression coefficients were then applied to window radiance observations to predict the emitted flux.

Gruber (1978) compared the flux computed in this way with wide angle flux measurements from the ERB experiment (Jacobowitz 1978) and showed the ERB data to be systematically higher by about 10 Wm^{-2}. As a consequence of this discrepancy, it was decided to review the model used in calculating flux data from window radiances, with particular emphasis on the following:

a. The inclusion of new information on atmospheric transmittance in the 11-μm window calculation of radiance.

b. The development of a nonlinear model to predict flux from radiance. This was necessary since the linear radiance-to-flux model leads to significant errors at both high and low flux values.

c. The method used to predict nadir radiance, R(0), from the radiance at nadir angle θ, R(θ).

As a result of this review, new models were developed. In the succeeding section we will describe their development and the application of the models to the NOAA satellite radiance observations.

2. TRANSMITTANCE COMPUTATIONS

Atmospheric transmittance for each of the 100 atmospheres and for six instrument 11-μm window filter profiles were calculated by Arking at NASA/GSFC. There were five filter profiles from the NOAA scanning radiometers and one from the TIROS-N Advanced Very High Resolution Radiometer (AVHRR). Arking's computer program calculates monochromatic transmittances to various pressure levels in the atmosphere. These are then convolved with the filter function to obtain the final filter transmittance function. The calculation is "exact" in that all the significant absorption lines are considered individually at each point on the wavenumber axis. The Lorentz profile is used at higher atmospheric pressures, and is replaced by the Voigt profile at pressures below 100 mb. For reasons of efficiency, Arking has condensed the scheme just described in his computer program. The accuracy of his streamlined approach, details of which have not yet been published, is comparable to that of the "exact" method outlined above.

A major feature of absorption in the 11-μm window is the effect of the water vapor continuum. The absorption is highly temperature sensitive. The original radiance calculations for the 100 atmospheres assumed a constant

absorption coefficient throughout the window region, and this may have been the single largest source of error in those calculations. In the present work, the data of Roberts et al. (1976), was used to define the continuum absorption. It was assumed that the continuum coefficients calculated at 880 cm^{-1} applied also at all wavenumbers transmitted by each filter.

Arking's results were defined at a fixed set of 40 atmospheric pressure levels. The 100 atmospheres were also defined at the same pressure levels, except that the surface (and cloud top) pressure could assume values which were not contained in the fixed set. For these cases, it was necessary to extrapolate or interpolate transmittance, temperature and water vapor mixing ratio. A monochromatic (far wing of a Lorentz line) model was used for the transmittance estimation; temperature and water vapor mixing ratio were extrapolated through an assumed linear dependence on the logarithm of pressure.

Radiance was calculated by numerical quadrature:

$$R = B_o\tau_o + \sum_{i=1}^{39} \overline{B_i}\,\Delta\tau_i \ , \qquad (1)$$

where the subscript o refers to the surface, and $\Delta\tau_i$ is the (positive) change in transmittance across layer i. $\overline{B_i}$ is the Planck function at the layer mean temperature.

The wavenumber at which $\overline{B_i}$ was calculated in (1) was given by

$$\nu = \nu_o + \gamma_1 T + \gamma_2 T^2 \ , \qquad (2)$$

where ν_o, γ_1, γ_2 are constants of regression calculated for each filter profile. The numerical values of γ_1 and γ_2 are small; ν differs from ν_o by less than 0.2 cm^{-1} at all tropospheric temperatures.

Transmittances and radiances were calculated at the following angles to the nadir; 0, 20, 40, 50, 60, 70, and 80 degrees. A planar stratified

atmosphere was assumed.

Figure 1 shows for the NOAA SR filter F 17

a. The present calculations (indicated by 100 crosses)

b. The best least squares linear fit to (i)

c. The original algorithm

d. A limiting curve defined by

$$F = \sigma T_{\nu_o}^4 , \tag{3}$$

where T_{ν_o} is the brightness temperature equivalent to the calculated radiance at wavenumber ν_o, and σ is Stefan's constant. For all atmospheres in which there is no inversion layer, the points in figure 1 must lie to the right of the limiting curve. A few of the atmospheric polar samples did contain strong surface inversion features, and these points lie just to the left of the limiting curve. The fact that the linear regression intersects the limiting curve at a substantial angle indicates that the regression line is inappropriate in this region. Even so, it is encouraging to note that the recalculated linear fit resulted in flux estimates 4% lower than those calculated from the original algorithm at high flux values, and that it increased low flux values by 1 to 2%, thus tending to reduce the discrepancies between flux estimates using the original algorithm and measurements from the Nimbus-6 ERB instrument.

3. REGRESSION MODEL

The present work has abandoned a regression between flux and radiance in favor of a regression between flux equivalent brightness temperature, T_F, and radiance equivalent brightness temperature, T_R. Temperature T_F is defined through eq. 3; T_R is evaluated at wavenumber ν_o.

The following quadratic form of the regression forces the curve through the origin (a physical boundary condition); a and b are constants of

regression

$$T_F = T_R\,(a + b\,T_R). \qquad (4)$$

Figures 2 and 3 show the form of the fit for the F 17 filter of the NOAA SR instruments. The standard deviation of the points about the fit in T_F is $1.7^{o}K$. Table 1 lists the regression constants for the NOAA series of satellites and for the AVHRR of TIROS-N.

The relation of the flux computed with the nonlinear algorithm (Fn) to that of the original linear model (Fo) is shown in figure 4, where the ratio ϕ = Fn/Fo is plotted on the abscissa and Fo on the ordinate. Except for a small range of values (170-250 WM^{-2}), the flux computed by the nonlinear model, Fn, is smaller than that computed from the linear model. The most rapid changes occur at flux values lower than 190 WM^{-2}. Above that value the change is much slower; the ratio of Fn/Fo decreasing to 0.9 at 380 WM^{-2} from 1.04 at 200 WM^{-2}.

4. CALCULATION OF NADIR RADIANCE

Figure 5 shows the change in calculated radiance as a function of view angle to the nadir for several extreme atmospheres selected from the set of 100. All the examples shown are for cloudless conditions. It is evident that prediction of R(0) from R(θ) becomes rapidly more inaccurate as θ increases. Examination of the complete set also shows that the dependence of R on θ is stronger for high values of R(0) than for low values. The following form was fitted to the complete set of data:

$$R(0) = R(\theta) + (\alpha_1 + \alpha_2\,R(\theta))(\sec\theta - 1) + (\beta_1 + \beta_2\,R(\theta))(\sec\theta - 1)^2 \qquad (5)$$

where α_1, α_2, β_1, β_2 are regression constants for each filter. Figure 6 shows the rms error of the R(0) predicted from R(θ) through equation (5). The rms

error in R(0) is below 1 mW $(m^2 st\ cm^{-1})^{-1}$, for θ below about 64^o (fig. 5). For a radiance of 100 mW $(m^2 st\ cm^{-1})^{-1}$, a 1% error in radiance corresponds to a brightness temperature error of about 0.7^oK. This is well below the 1.7^oK standard deviation of the fitted points about the curve of eq. (4). The error in flux estimation for all probable satellite view angles will therefore be dominated by the accuracy of the primary equation (eq. 4), and not by the accuracy of eq. (5).

Table 2 gives the relevant constants for the 6 radiometers involved.

A comparison between the model computation of eq. (5) and the previously used limb corrections are shown in figure 7. The temperature correction (ΔT) is plotted against observed temperature for three different satellite zenith angles. The results of eq. (5) show somewhat less temperature correction than previously applied. However, the maximum difference in the correction is 0.5^oK and occurs at high temperatures and large zenith angles. For all practical purposes, this difference is not significant.

5. A COMPARISON OF THE NEW ALGORITHM WITH THE ORIGINAL

The new and old algorithms were compared by examining profiles of zonal averaged flux data and mapped fields of the flux values for a 7-day test period, July 19-25, 1977. The results are shown in figures 8 and 9 which present the original flux computations (F_o) and the difference between the new algorithm and the old algorithm ($F_n - F_o$), respectively. Examination of those figures indicate compatibility with the theoretical and modeling computations presented in figures 2 and 4. What is of interest is the location and distribution of the corrections. Thus, we observe the largest corrections to be in the South Polar region because of the low flux values that occur there ($F_o < 160\ Wm^{-2}$). Large differences also occur close to 30^oN and about 10^oS because of the few clouds and resulting high flux. The difference at 30^oN is

greater than at 10^{o}S; most likely it is a manifestation of the shift of the subtropical highs northward during this season and the declination of the Sun (approximately 21^{o}).

There are two areas of positive differences, small in magnitude and area. Those are the regions where the outgoing flux is between 170 and 250 Wm^{-2}.

It is to be expected that this pattern will shift somewhat with season, but it is reasonable to conclude that on the average the nonlinear model for computing flux will result in lower flux values than previously derived. An estimate of just how much, will be presented later.

The spatial distribution of the differences are shown in figure 10. Large differences (some in excess of 20 Wm^{-2}) are observed over the warm subtropical deserts and cloud-free ocean areas. Large differences are also observed over Antarctica, which is due to the low temperatures during this time of year.

6. A SIMPLIFIED APPLICATION OF THE NEW MODEL

We decided to recompute flux values derived from scanning radiometer data according to the new method. Since the data available from the SR covered several years of operation, this project represented a large computing task. For a single radiance observation, the function ϕ of figure 4 should be applied to each high resolution radiance observation, but this would require computations to be performed on the mapped data base, and would be extremely expensive. We chose instead to perform the corrections on the daily flux values, computed by the old method, and archived every 2.5^{o} of latitude and longitude (Gruber 1978). These daily values are the result of an averaging and smoothing operation on the high resolution mapped data base, and correcting them with the function shown in figure 4 introduces an error into the recalculated flux values since the old algorithm and new algorithm are not linearly related.

An assessment of the errors introduced by this procedure was made using the test sample of data from July 1977. High resolution flux data were computed using the new algorithm, averaged and mapped to 2.5° latitude-longitude arrays and then averaged for the 7-day period. Then correction factors were applied to the daily 2.5° latitude-longitude flux values computed from the old method.

Figure 11 shows the difference between the two methods ("exact" minus "simplified") for zonal average flux values. The differences are seen to be less than 2 Wm^{-2}, with the largest difference occurring at 10°N, approximately in the ITCZ region. The spatial distribution of the error is shown in figure 12. There we see small areas with errors as large as 3 Wm^{-2} also located in the ITCZ region. These errors are less than the standard error of the original (i.e., linear) flux estimation procedure which was about 5 Wm^{-2}. It was therefore decided to apply the simplified corrections to the entire record (June 1974 - February 1978) of daily flux computations.

Figure 13 shows the results of applying this model to zonally averaged data for July 1976. Profiles obtained from ERB and the original method are shown along with the adjusted flux values. The adjusted globally averaged flux shows a decrease of about 1.5% (from 254.8 to 250.9 Wm^{-2}), not a dramatic amount. However, as seen in figure 13, nearly all of that change comes from the subtropical high pressure belts of each hemisphere. For example, the change at 25°N is 3.2% and at 15S, 2.6%, nearly twice the globally averaged change. Notice that because of the concentration of the difference in the subtropics, the north-south gradient is decreased.

The spatial distribution of the differences are shown in figure 14. The largest adjustments are made over the hot deserts of North Africa and the low temperature areas of Antarctica, in accordance with the previous discussion.

The percentage change in those areas are considerably larger, being as high as 10% in Antarctica and about 6% over the hottest parts of the subtropical deserts of North Africa.

7. CONCLUDING REMARKS

A rationale has been presented for adjusting the linear model used to estimate total flux from 10-12 μm window radiance. As a result of the analysis, a new nonlinear regression model has been derived. Analysis of the results indicate a small precentage change on an integrated global basis. However, since this change is not uniformly distributed across the globe, use of the nonlinear model results in some significant differences. Primary among them is the large decrease in outgoing longwave radiation in the subtropical regions. This results in greater surpluses or smaller deficits in net radiation than previously calculated for those areas.

REFERENCES

Gruber, A., 1977: Determination of the Earth-atmosphere radiation budget from NOAA satellite data. NOAA Technical Report NESS 76, 28 pp.

Smith, W. L., J. Hickey, Hugh B. Howell, H. Jacobowitz, Don T. Hilleary, and A. J. Drummond, 1977: Nimbus 6 Earth radiation budget experiment, Applied Optics, 16, pp. 306-318.

Roberts, R. E., J. E. A. Selby, and L. M. Biberman, 1976: Infrared Continuum Absorption by Atmospheric Water Vapor in the 8-12 μm window, Applied Optics, 15, 2085-2090.

Wark, D. Q., G. Yamamoto, and J. Lienesch, 1962: Infrared flux and surface temperature determinations from TIROS radiometer measurements. Meteorological Satellite Laboratory Report No. 10, U. S. Department of Commerce, Weather Bureau, Washington, D. C.

Table 1.--Radiance-to-flux regression constants derived for scanning radiometer filters

Filter	$\nu_o(cm^{-1})$	a	$b(K^{-1})$
TIROS-N AVHRR	912.63	1.3203	-.001397
NOAA SR F17	879.69	1.3210	-.001396
NOAA SR F15	873.09	1.3208	-.001397
NOAA SR F12	868.82	1.3195	-.001393
NOAA SR F21	869.06	1.3185	-.001387
NOAA SR F22	871.14	1.3197	-.001392

Table 2.--Limb darkening regression constants derived for scanning radiometer filters

Filter	α_1(mW etc.)	α_2	β_1(mW etc.)	β_2
TIROS-N AVHRR	-2.301	.04767	.1244	-.002096
NOAA SR F17	-2.537	.04949	.1412	-.002271
NOAA SR F15	-2.554	.04838	.1420	-.002212
NOAA SR F12	-2.557	.04763	.1437	-.002222
NOAA SR F21	-2.643	.05008	.1512	-.002404
NOAA SR F22	-2.621	.04986	.1480	-.002324

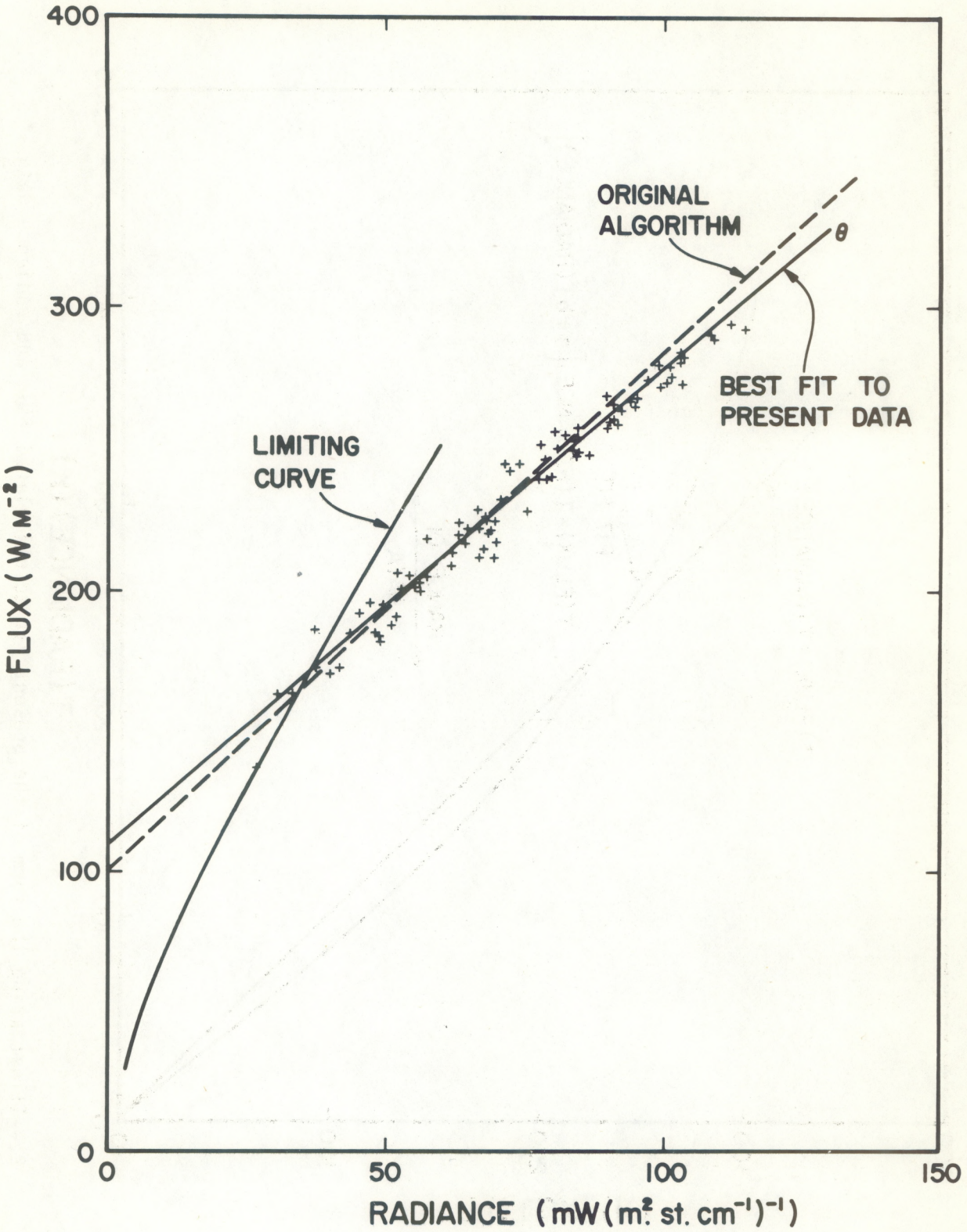

1.--A comparison between the original radiance-to-flux algorithm and the present method of calculation

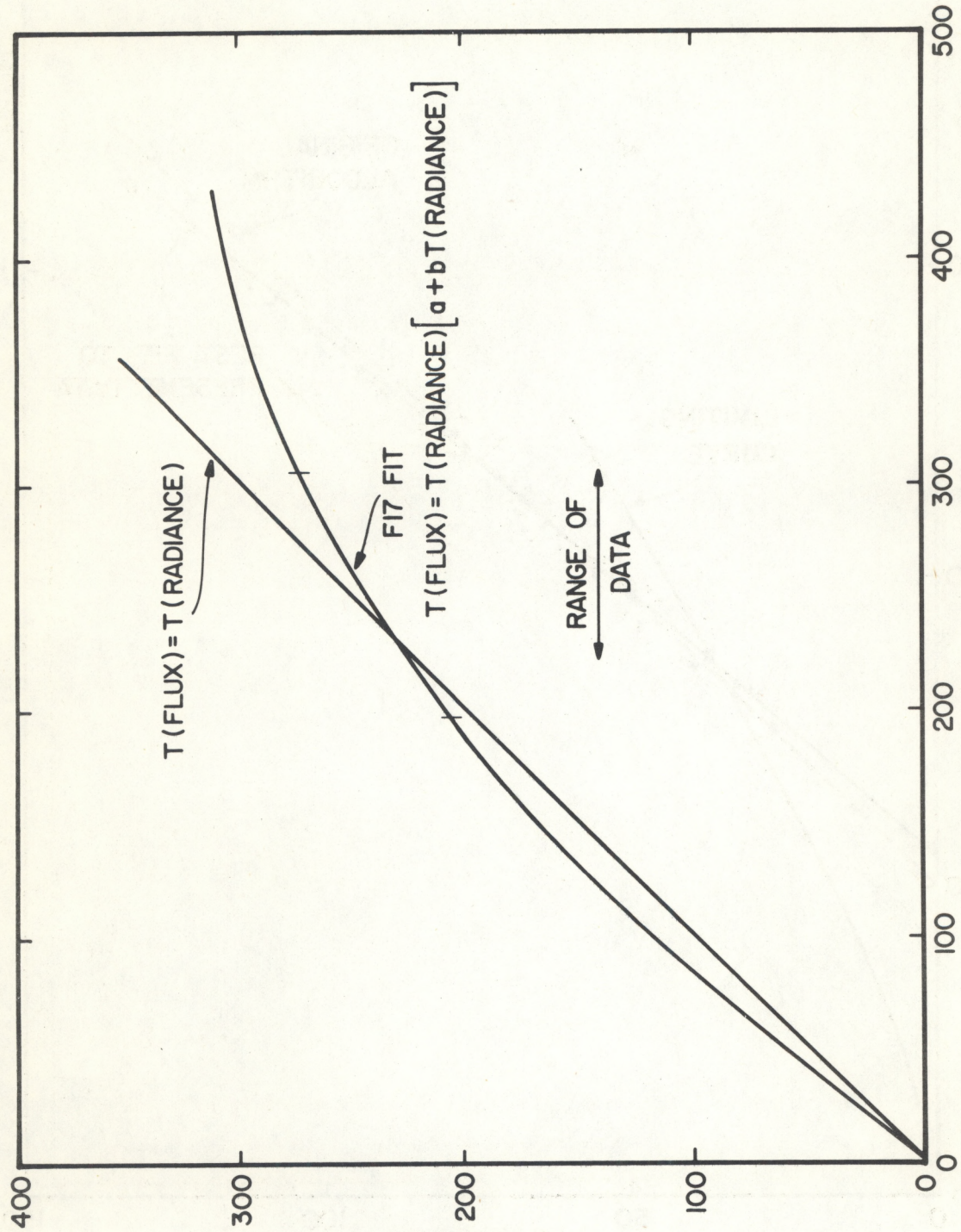

2.--Illustrating the form of the present fit to calculated flux and radiance data

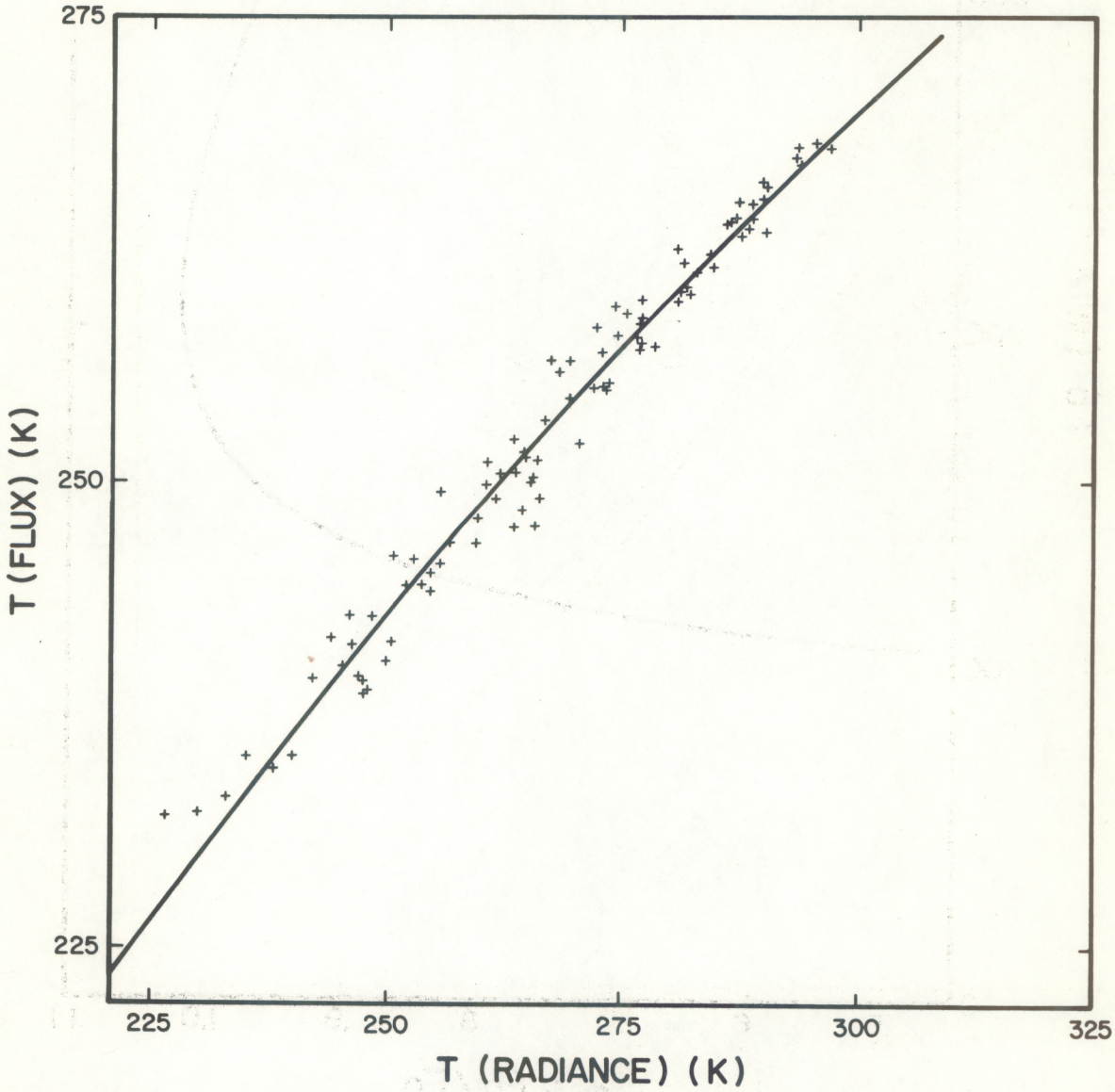

3.--Calculated data set and the present fit

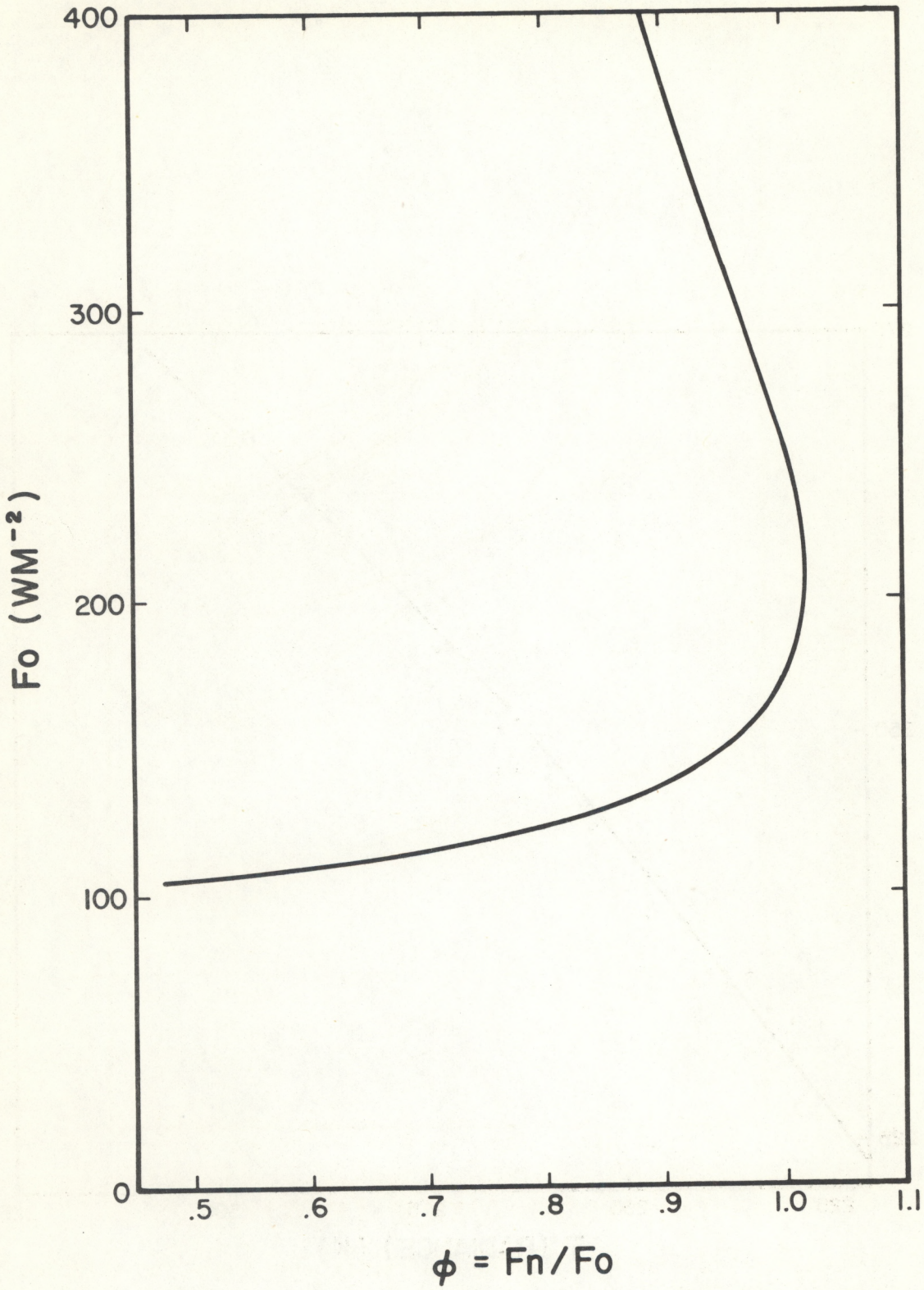

4.--The ratio (ϕ) of fluxes calculated from the nonlinear (Fn) and original (Fo) methods, expressed as a function of Fo

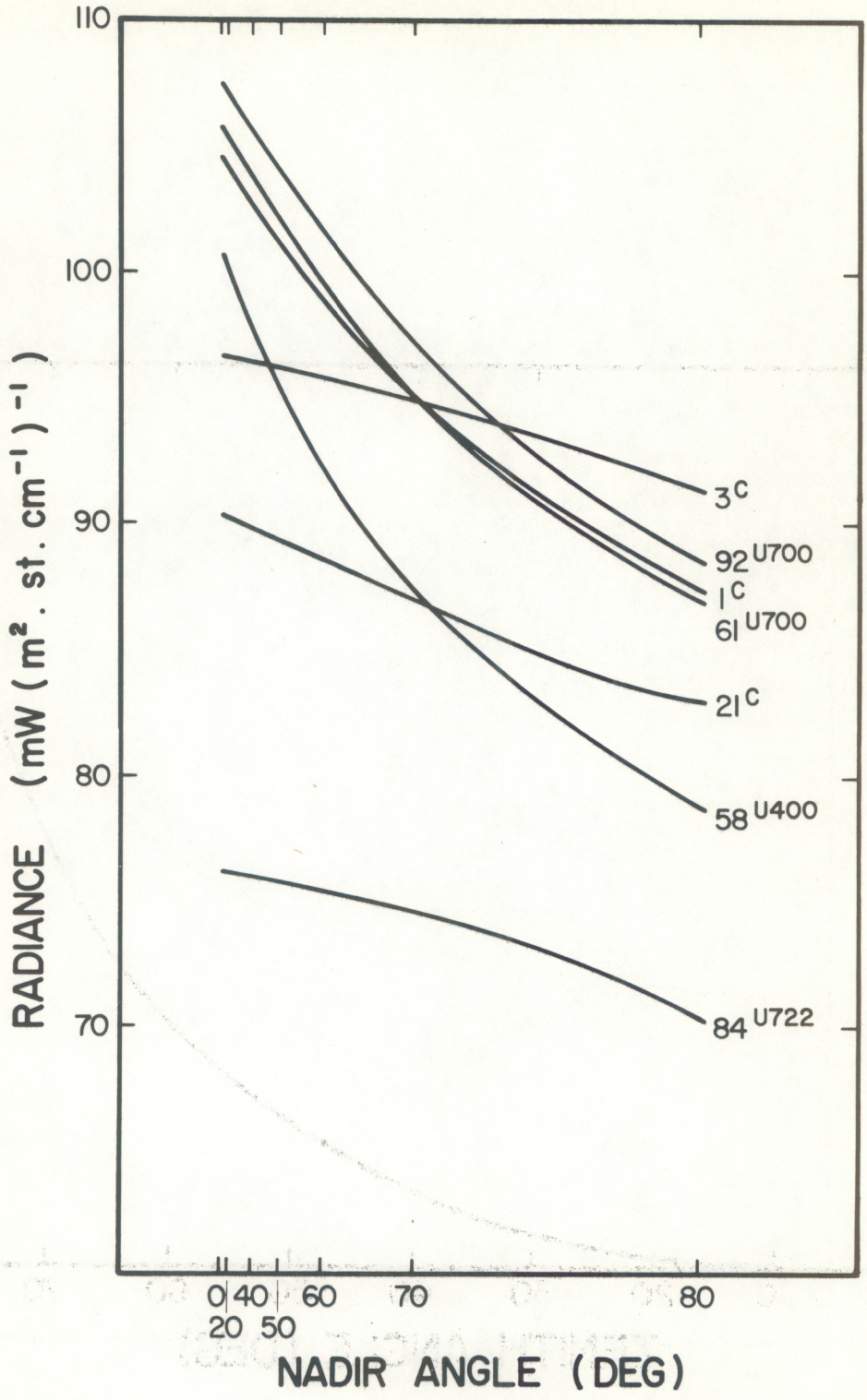

5.--Calculated radiance as a function of nadir view angle for selected cases. The initial number is the atmospheric case number (1-106): "C" indicates a clear atmosphere. "U" indicates undercast, and is followed by the assumed cloud top pressure

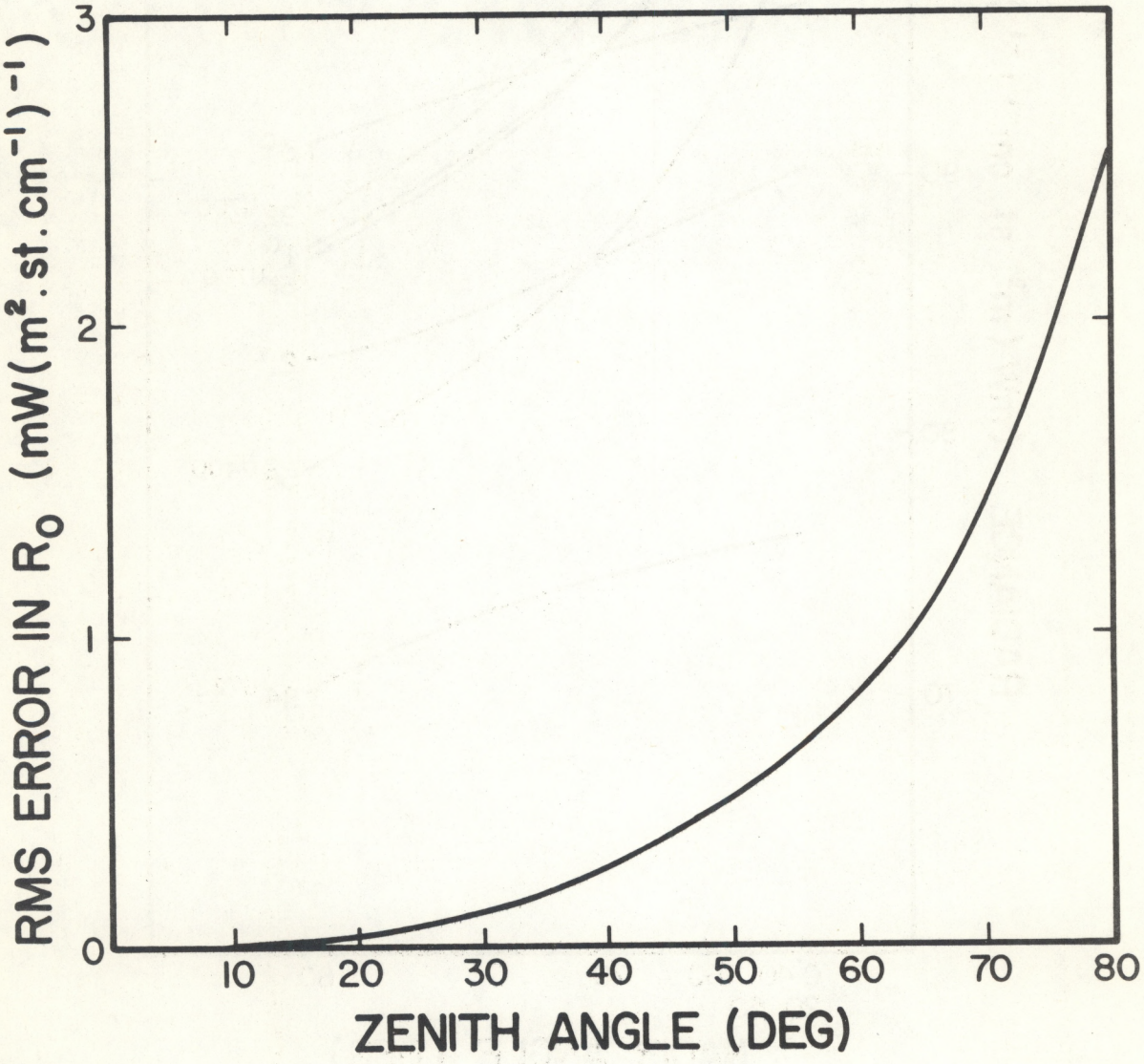

6.--Rms error in derived nadir radiance as a function of the nadir angle at which radiance was measured

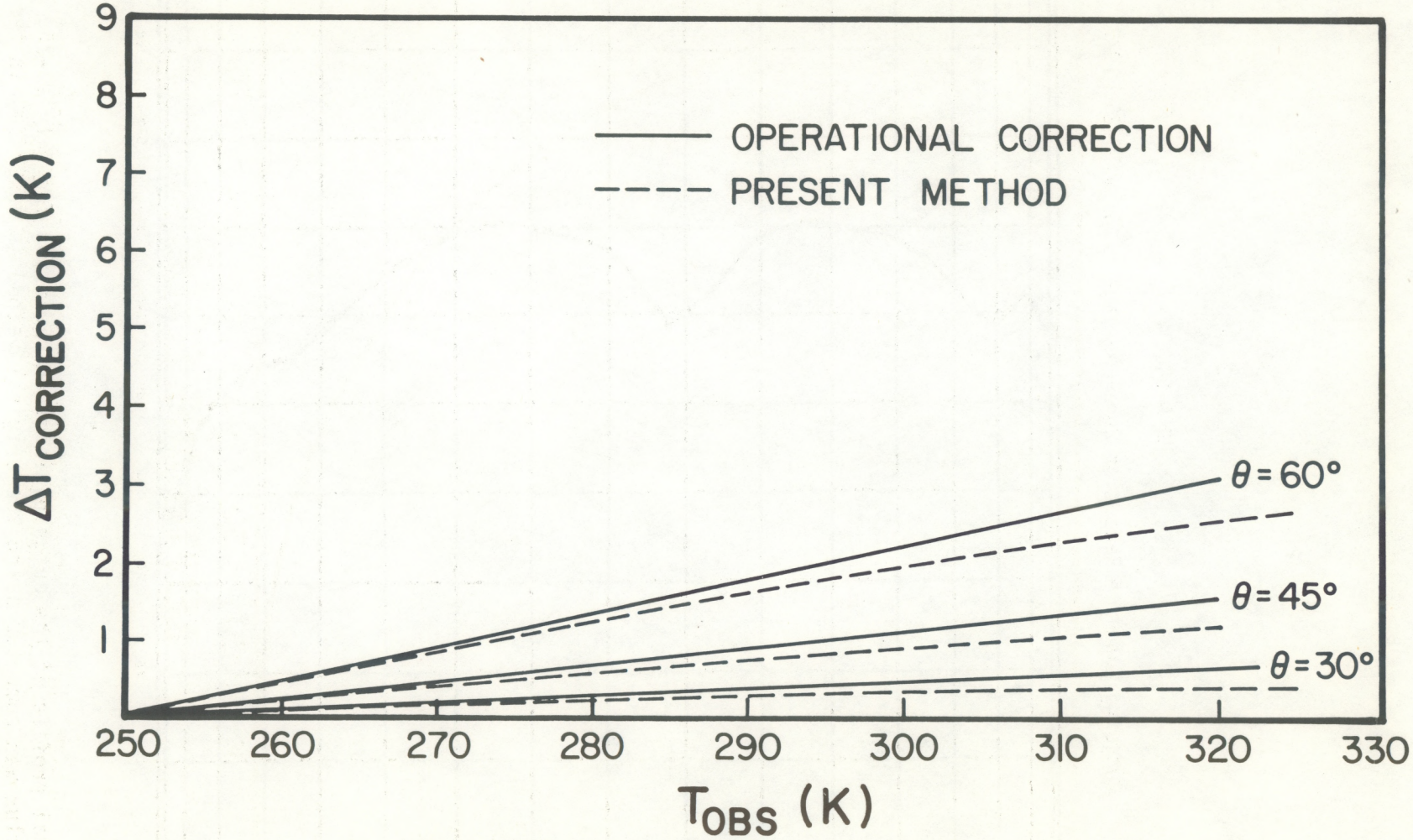

7--A comparison between the NESS operational limb correction (solid) and the derived limb correction (dashed)

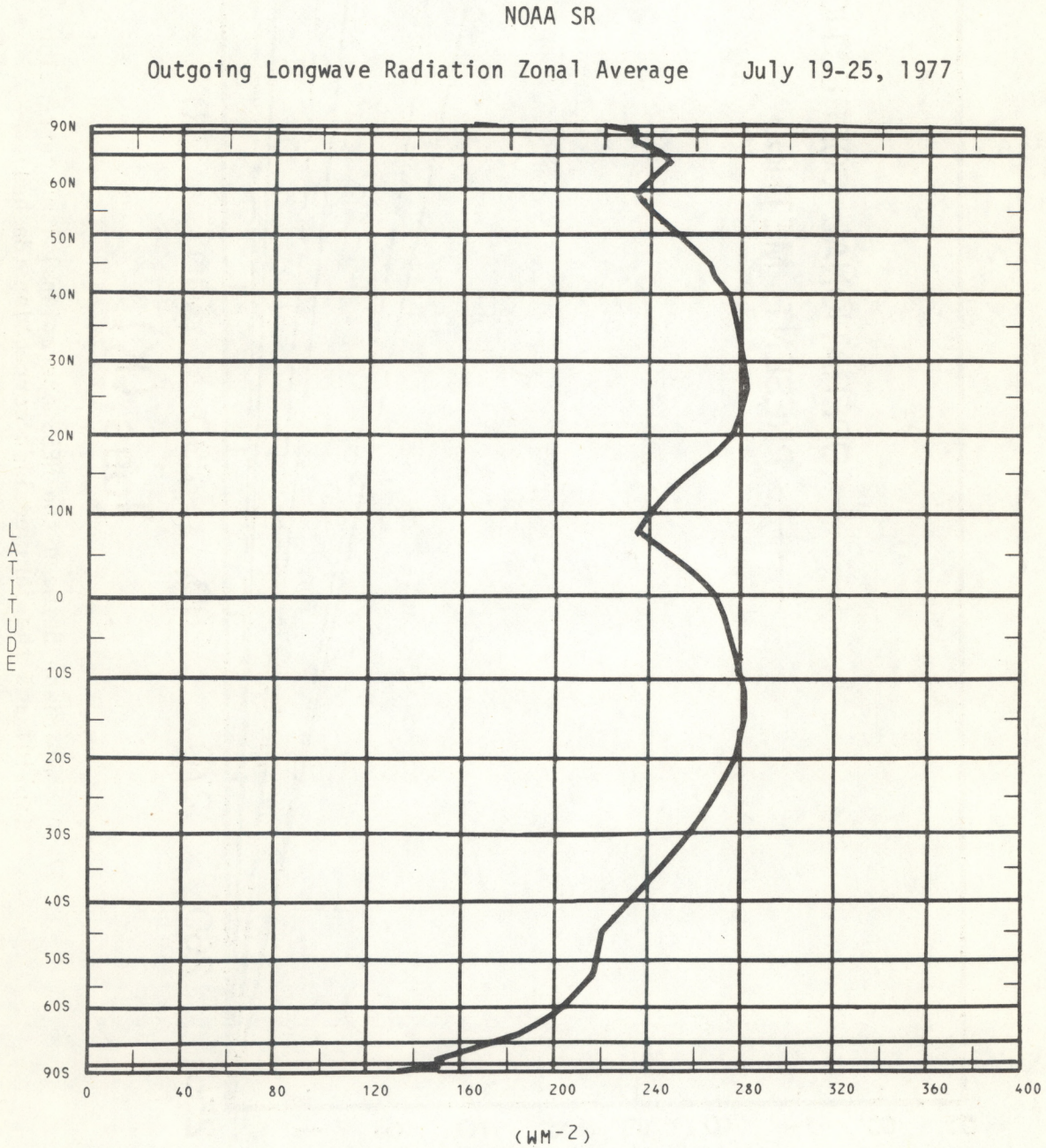

8.--A zonal profile of the outgoing longwave radiation for July 19-25, 1977. The flux was computed using the original method as described in the text.

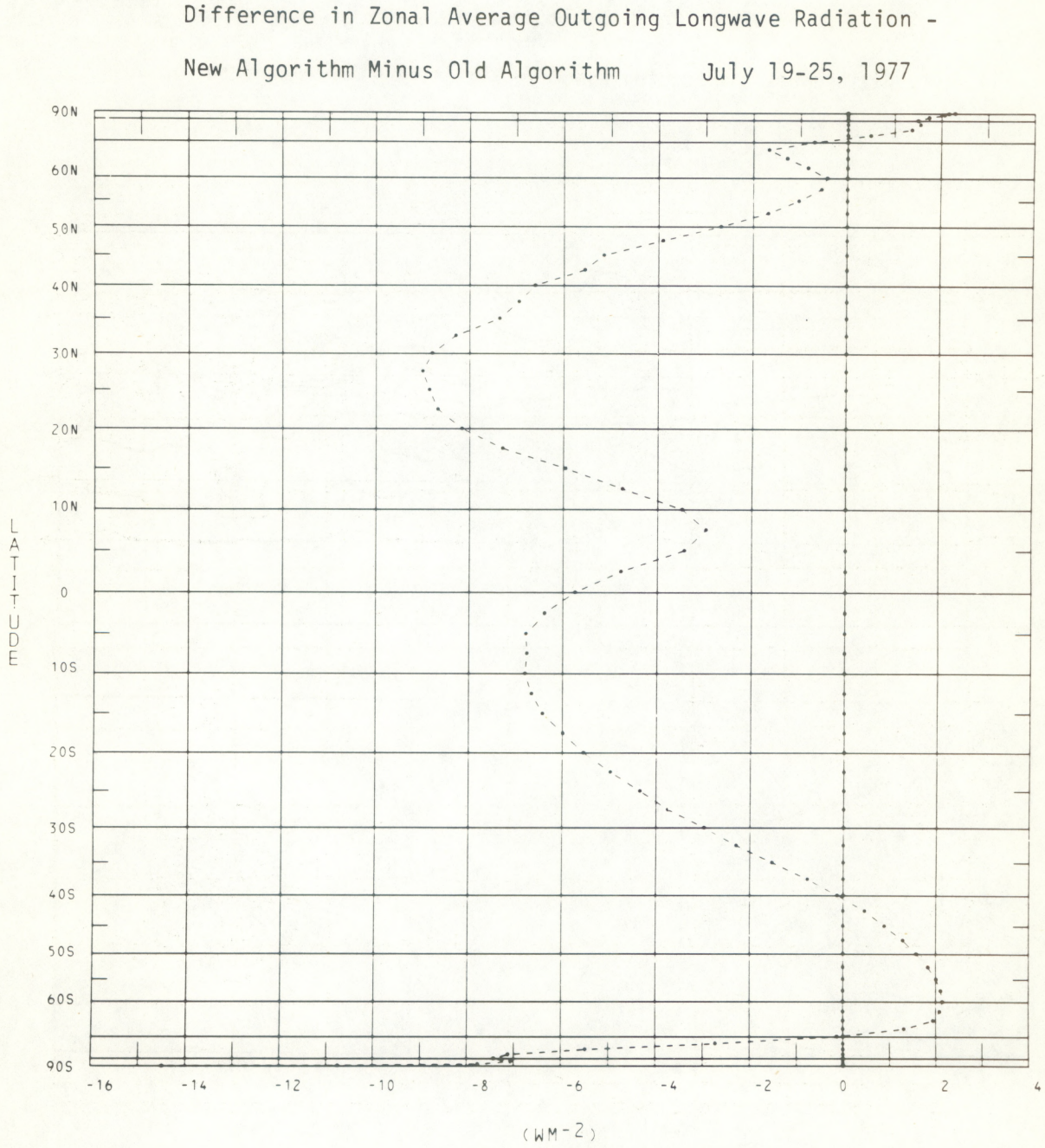

9.--Zonal profiles of the outgoing longwave radiation computed by the new method (Fn) minus that computed by the original method (Fo), averaged for the period July 19-25, 1977

Differences in Outgoing Longwave Radiation - New Algorithm

Minus Original Algorithm July 19-25, 1977

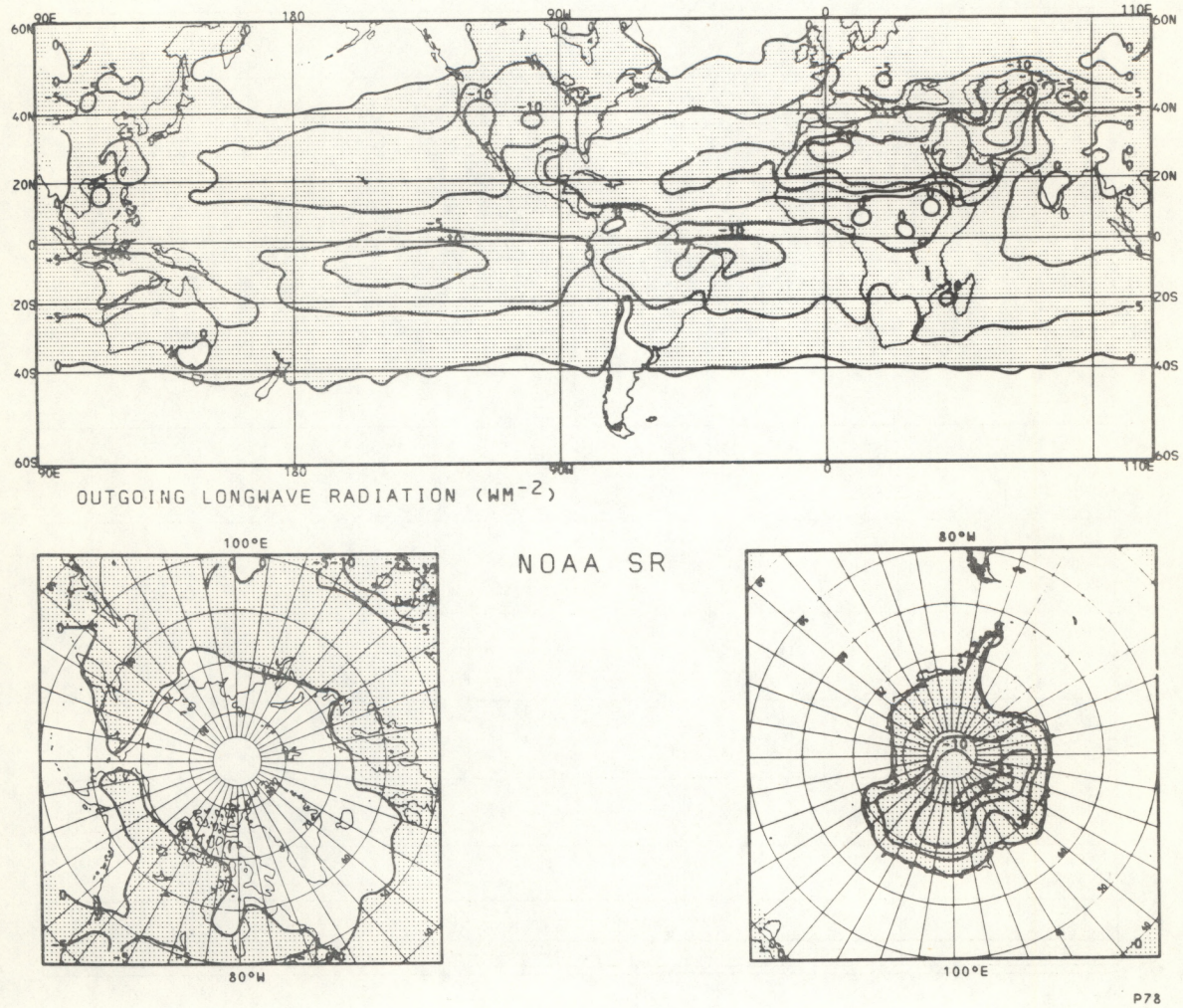

10.--Spatial distribution of the average outgoing longwave radiation computed by the new method (Fn) minus that computed by the original method (Fo) for July 19-25, 1977

Difference in Zonal Average Outgoing Longwave Radiation -

"Exact" minus "Simplified" July 19-25, 1977

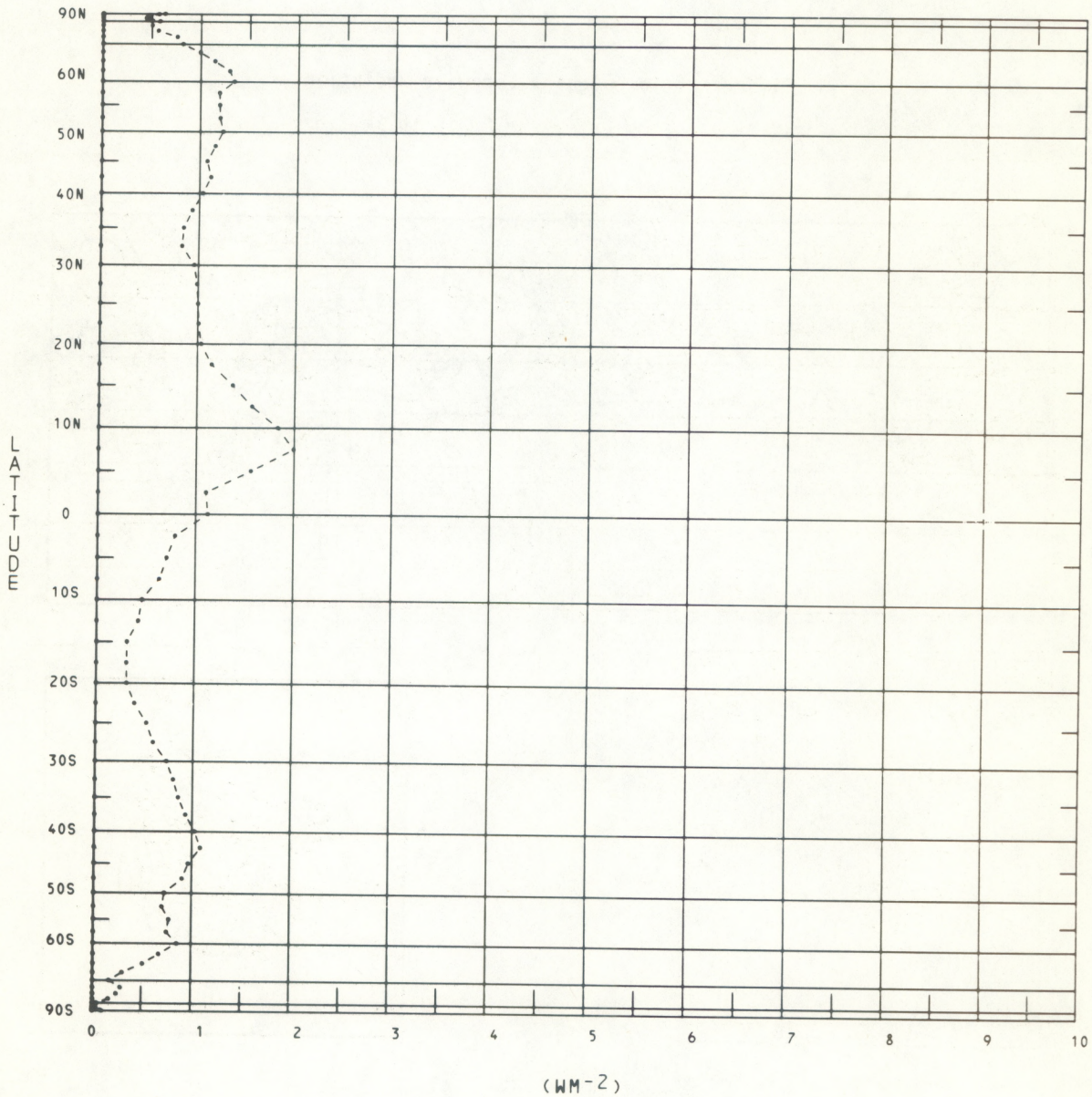

11.--Zonal profile of the outgoing longwave radiation computed by the "exact" method minus that computed by the "simplified" method, for July 19-25, 1977. See text.

Difference in Outgoing Longwave Radiation -

"Exact" minus "Simplified" July 19-25, 1977

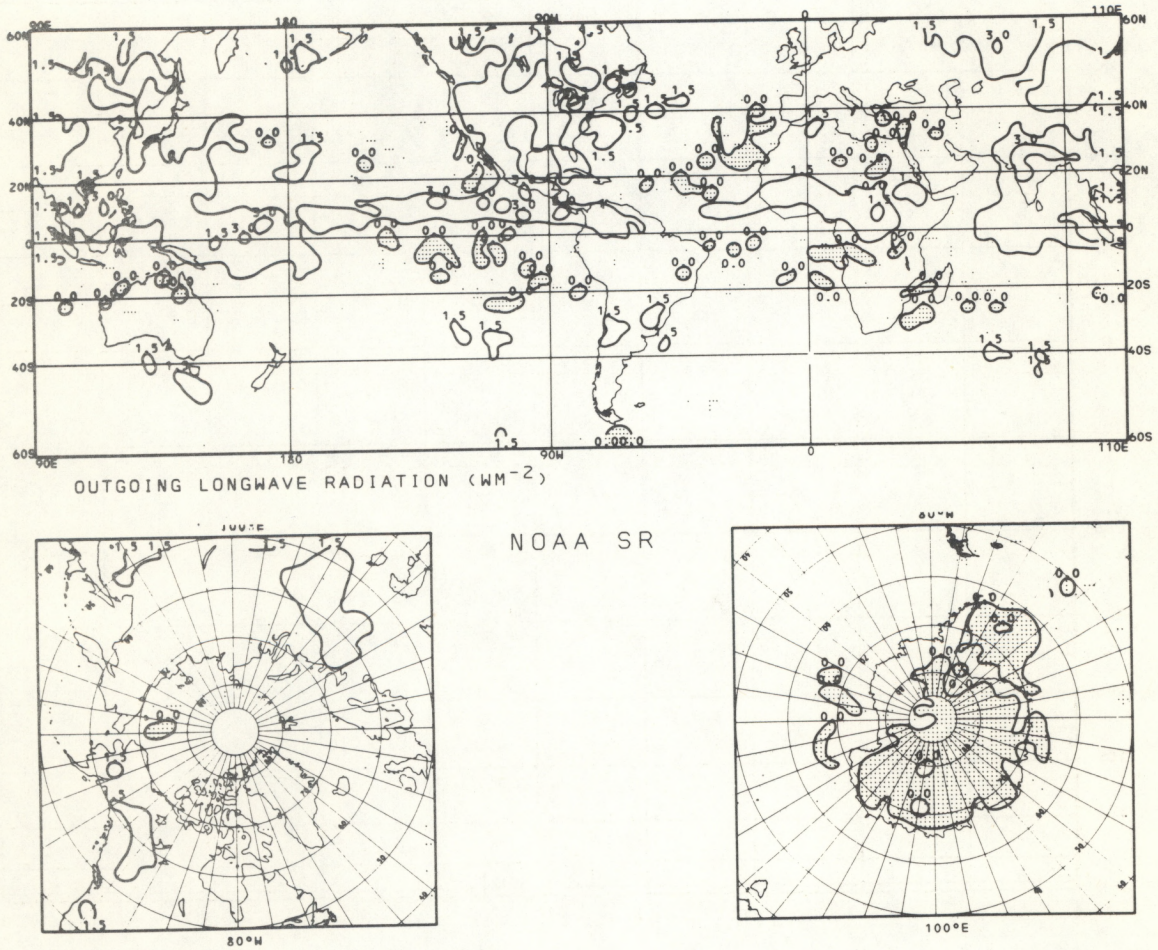

12.--Spatial distribution of the outgoing longwave radiation by the "exact" method minus that computed by the simplified method, for July 19-25, 1977

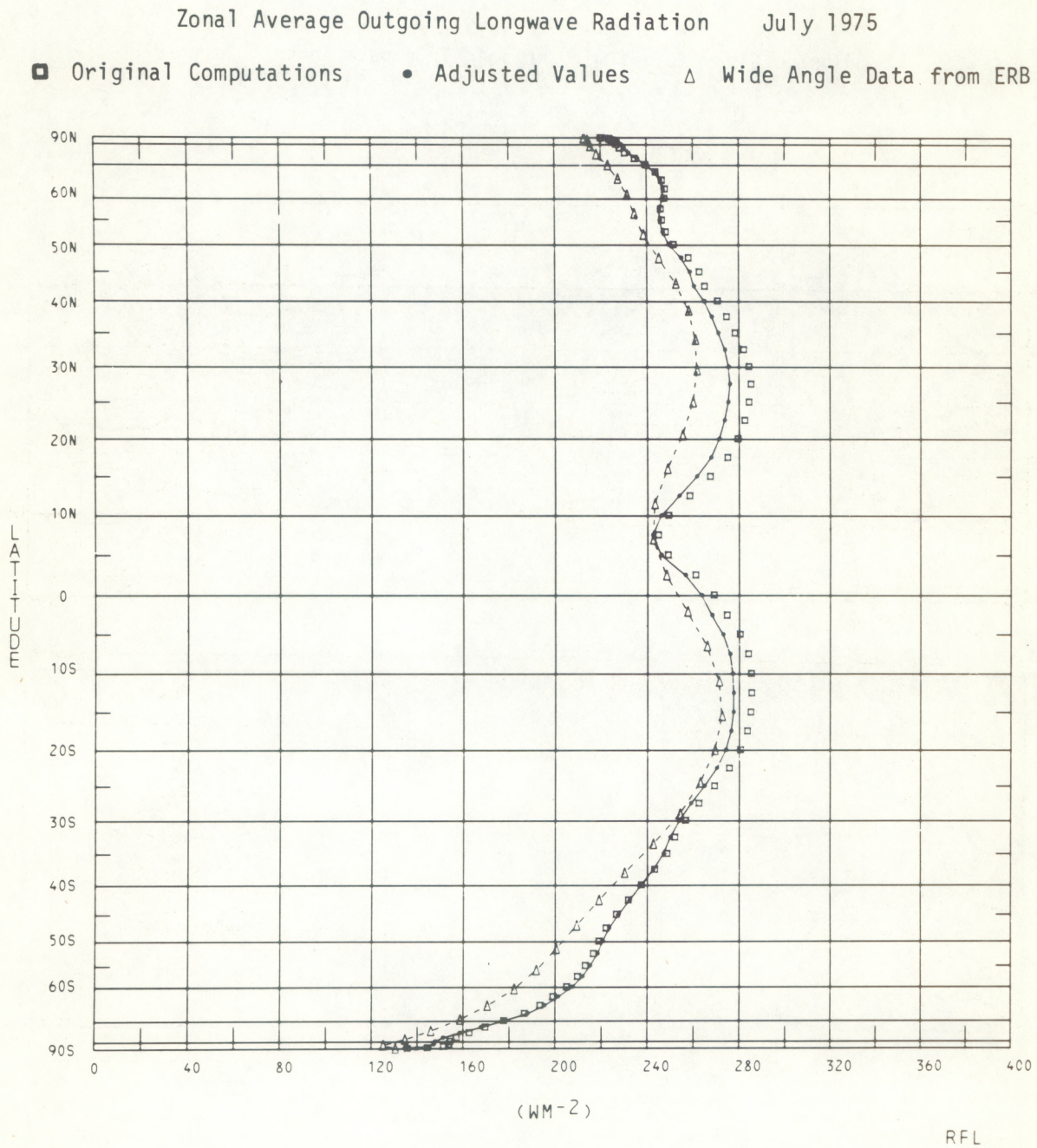

13.--A comparison of zonal profiles of outgoing longwave radiation computed from the Earth Radiation Budget (ERB) experiment on Nimbus 6, the original method and the simplified method, for July 1976

Adjusted Computations minus Original Computations July 1976

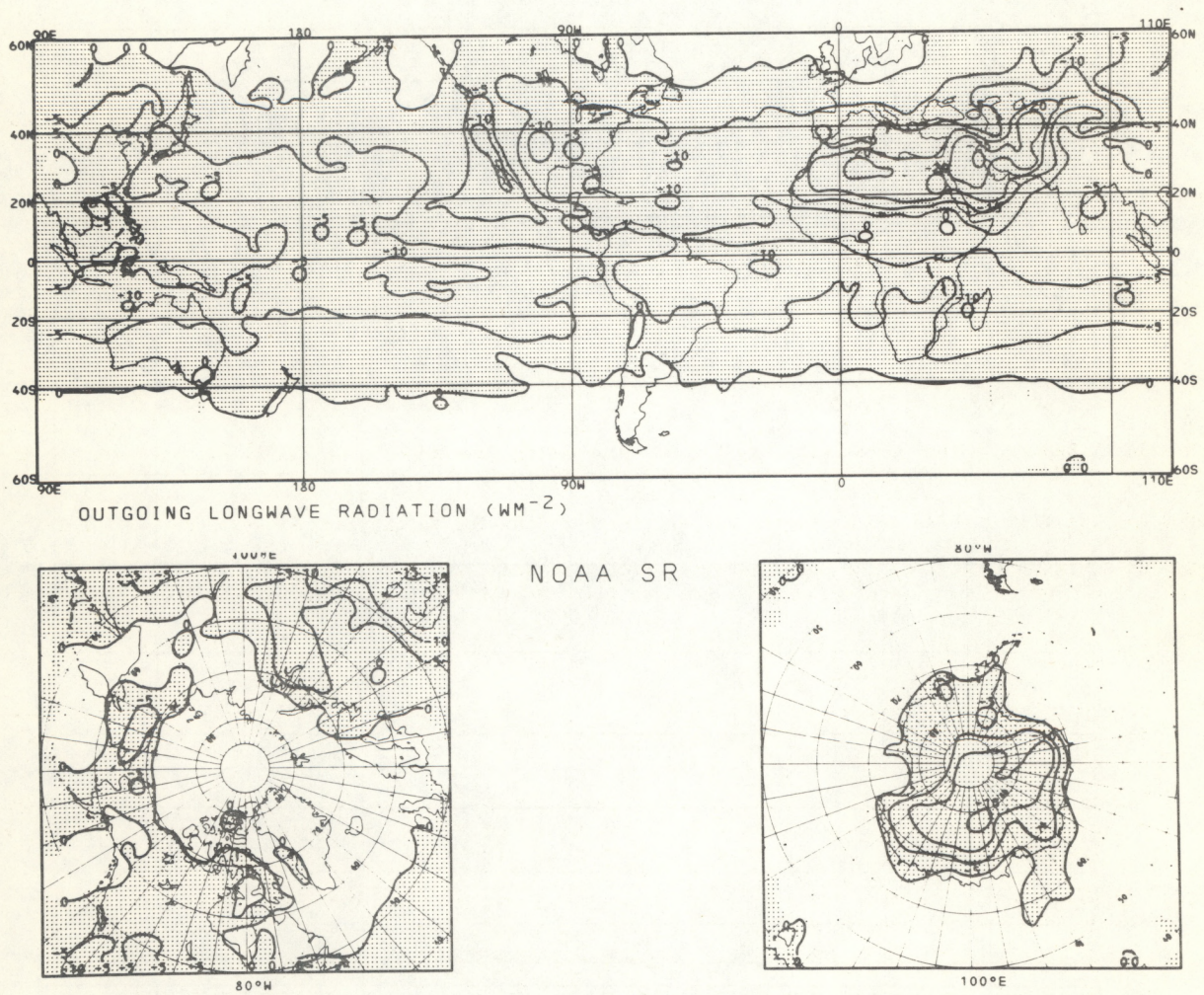

14.--Spatial distribution of the outgoing longwave radiation computed by the original method minus that computed by the simplified method for July 1976

(Continued from inside front cover)

NESS 82 The GOES Data Collection System Platform Address Code. Wilfred E. Mazur, Jr., October 1976, 26 pp. (PB-261-968/AS)

NESS 83 River Basin Snow Mapping at the National Environmental Satellite Service. Stanley R. Schneider, Donald R. Wiesnet, and Michael C. McMillan, November, 1976, 19 pp. (PB-263-816/AS)

NESS 84 Winter Snow-Cover Maps of North America and Eurasia From Satellite Records, 1966-1976. Michael Matson, March 1977, 28 pp. (PB-267-393/AS)

NESS 85 A Relationship Between Weakening of Tropical Cyclone Cloud Patterns and Lessening of Wind Speed. James B. Lushine, March 1977, 12 pp. (PB-267-392/AS)

NESS 86 A Scheme for Estimating Convective Rainfall From Satelliue Imagery. Roderick A. Scofield and Vincent J. Oliver, April 1977, 47 pp. (PB-270-762/AS)

NESS 87 Atlantic Tropical and Subtropical Cyclone Classifications for 1976. D. C. Gaby, J. B. Lushine, B. M. Mayfield, S. C. Pearce, K.O. Poteat, and F. E. Torres, April 1977, 13 pp. (PB-269-674/AS)

NESS 88 National Environmental Satellite Service Catalog of Products. Dennis C. Dismachek (Editor), June 1977, 102 pp. (PB-271-315/AS)

NESS 89 A Laser Method of Observing Surface Pressure and Pressure-Altitude and Temperature Profiles of the Troposphere From Satellites. William L. Smith and C. M. R. Platt, July 1977, 38 pp. (PB-272-660/AS)

NESS 90 Lake Erie Ice: Winter 1975-76. Jenifer H. Wartha, August 1977, 68 pp. (PB-276-386/AS)

NESS 91 In-Orbit Storage of NOAA-NESS Standby Satellites. Brtce Sharts and Chris Dunker, September 1977, 3 pp. (PB-283-078/AS)

NESS 92 Publications and Final Reports on Contracts and Grants, 1976. Catherine M. Frain (Compiler), August 1977, 11 pp. (PB-273-169/AS)

NESS 93 Computations of Solar Insolation at Boulder, Colorado. Joseph H. Pope, September 1977, 13 pp. (PB-273-679/AS)

NESS 94 A Report on the Chesapeake Bay Region Nowcasting Experiment. Roderick A. Scofield and Carl E. Weiss, December 1977, 52 pp. (PB-277-102/AS)

NESS 95 The TIROS-N/NOAA A-G Satellite Series. Arthur Schwalb, March 1978, 75 pp. (PB-283-859/AS)

NESS 96 Satellite Data Set for Solar Incoming Radiation Studies. J. Dan Tarpley, Stanley R. Schneider, J. Emmett Bragg, and Marshall P. Waters, III, May 1978, 36 pp. (PB-284-740/AS)

NESS 97 Publications and Final Reports on Contracts and Grants, 1977. Catherine M. Frain (Compiler), August 1978, 13 pp. (PB-287-855/AS)

NESS 98 Quantitative Measurements of Sea Surface Temperature at Several Locations Using the NOAA-3 Very High Resolution Radiometer. Laurence Breaker, Jack Klein, and Michael Pitts, September 1978, 28 pp. (PB-288-488/AS)

NESS 99 An Empirical Model for Atmospheric Transmittance Functions and Its Application to the NIMBUS-6 HIRS Experiment. P.G. Abel and W.L. Smith, NESS, and A. Arking, NASA, September 1978, 29 pp. (PB-288-487/AS)

NESS 100 Characteristics and Environmental Properties of Satellite-Observed Cloud Rows. Samuel K. Beckman (in consultation).

NESS 101 A Comparison of Satellite Observed Middle Cloud Motion With GATE Rawinsonde Data. Leroy D. Herman, January 1979, 13 pp. (PB-292-341/AS)

NESS 102 Computer Tracking of Temperature-Selected Cloud Patterns. Lester F. Hubert, January 1979, 15 pp. (PB-292-159/AS)

NESS 103 Objective Use of Satellite Data To Forecast Changes in Intensity of Tropical Disturbances. Carl O. Erickson, April 1979, 44 pp. (PB-298-915)

NESS 104 Publications and Final Reports on Contracts and Grants. Catherine M. Frain, (Compiler), September 1979.

NESS 105 Optical Measurements of Crude Oil Samples Under Simulated Conditions. Warren A. Hovis and John S. Knoll, October 1979, 20 pp.

NOAA SCIENTIFIC AND TECHNICAL PUBLICATIONS

The National Oceanic and Atmospheric Administration was established as part of the Department of Commerce on October 3, 1970. The mission responsibilities of NOAA are to assess the socioeconomic impact of natural and technological changes in the environment and to monitor and predict the state of the solid Earth, the oceans and their living resources, the atmosphere, and the space environment of the Earth.

The major components of NOAA regularly produce various types of scientific and technical information in the following kinds of publications:

PROFESSIONAL PAPERS — Important definitive research results, major techniques, and special investigations.

CONTRACT AND GRANT REPORTS — Reports prepared by contractors or grantees under NOAA sponsorship.

ATLAS — Presentation of analyzed data generally in the form of maps showing distribution of rainfall, chemical and physical conditions of oceans and atmosphere, distribution of fishes and marine mammals, ionospheric conditions, etc.

TECHNICAL SERVICE PUBLICATIONS — Reports containing data, observations, instructions, etc. A partial listing includes data serials; prediction and outlook periodicals; technical manuals, training papers, planning reports, and information serials; and miscellaneous technical publications.

TECHNICAL REPORTS — Journal quality with extensive details, mathematical developments, or data listings.

TECHNICAL MEMORANDUMS — Reports of preliminary, partial, or negative research or technology results, interim instructions, and the like.

Information on availability of NOAA publications can be obtained from:

ENVIRONMENTAL SCIENCE INFORMATION CENTER (D822)
ENVIRONMENTAL DATA AND INFORMATION SERVICE
NATIONAL OCEANIC AND ATMOSPHERIC ADMINISTRATION
U.S. DEPARTMENT OF COMMERCE

6009 Executive Boulevard
Rockville, MD 20852

NOAA--S/T 79-277